Supplementary Information for

Elastic strain controlling the activity and selectivity of CO_2 electroreduction on Cu overlayers

Minshu Du[*ab], Xin Zhao[c], Geju Zhu[a], Hsien-Yi Hsu[de] and Feng Liu[*af]

[a] School of Materials Science and Engineering, Northwestern Polytechnical University, Xi'an 710072, Shaanxi, China

[b] Yangtze River Delta Research Institute of NPU, Taicang 215400, Jiangsu, China

[c] School of Materials Science and Chemical Engineering, Xi'an Technological University, Xi'an 710021, Shaanxi, China

[d] School of Energy and Environment & Department of Materials Science and Engineering, City University of Hong Kong, Kowloon Tong, Hong Kong, China

[e] Shenzhen Research Institute of City University of Hong Kong, Shenzhen 518057, P.R. China

[f] Analytical & Testing Center, Northwestern Polytechnical University, Xi'an 710072, Shaanxi, China

Table S1. Calculated the deposited charge *Q* and thickness *d* of Cu overlayers

Deposition Potential *E* (V vs. RHE)	**Deposition time *t* (s)**	***Q*** **(C)**	**Thickness *d* (nm)**	**Geometric area *s* (cm^2)**
0.015	3	5.52×10^{-3}	5	0.4
0.015	20	3.47×10^{-2}	32	0.4

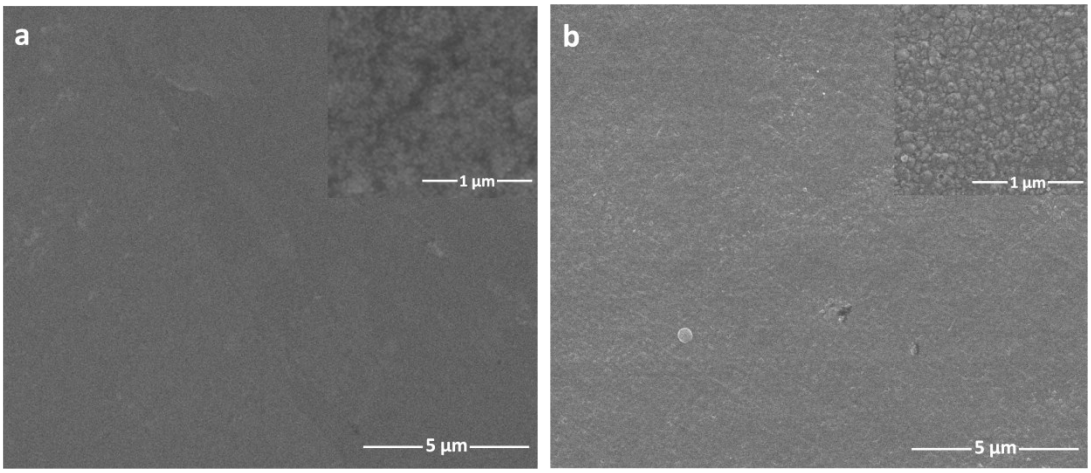

Figure S1. SEM images of the (a) 5 nm Cu and (b) 32 nm Cu overlayers deposited on NiTi substrate to show the surface morphology of nanofilm. The morphology details were also shown with higher magnification as inserted.

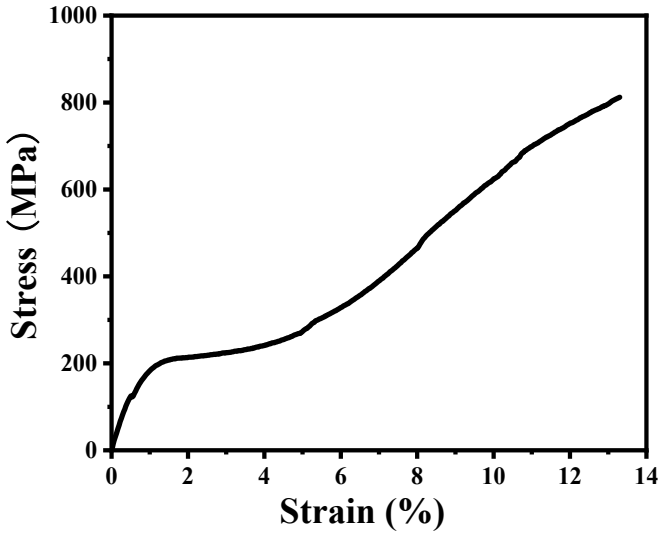

Figure S2. Engineering stress-strain curve of NiTi shape memory alloy at the room temperature for its two-way shape memory effect training.

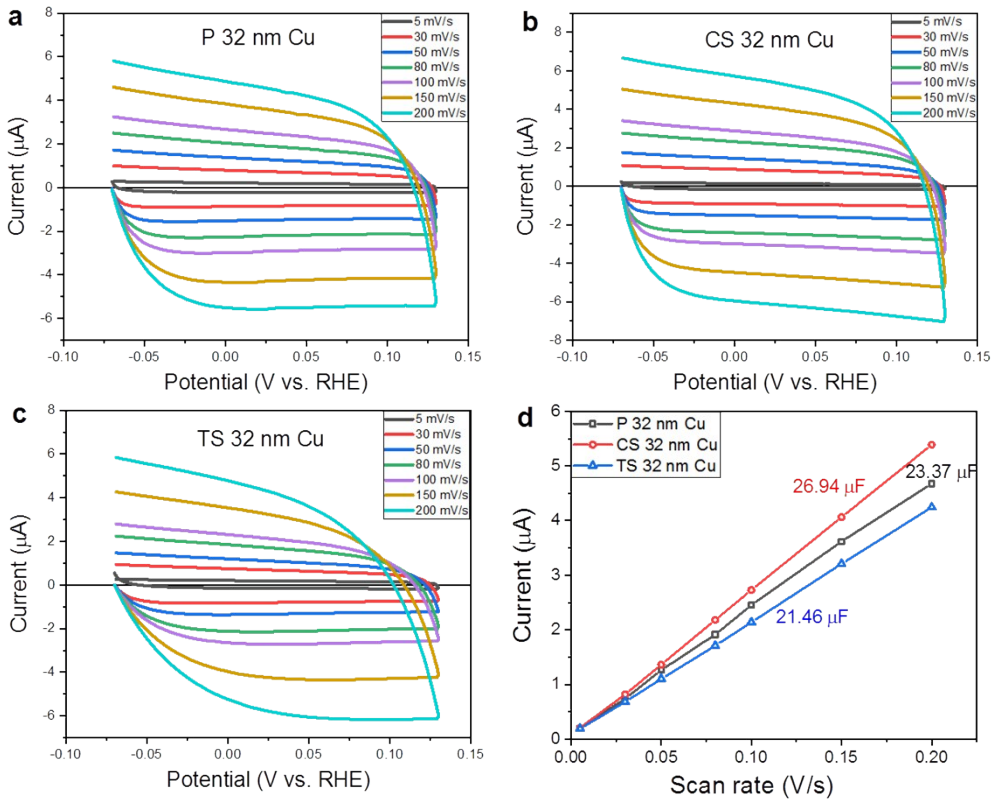

Figure S3. Double-layer capacitance measurements for determining the electrochemical active surface area for three state 32 nm Cu overlayers from voltammetry in CO_2 saturated 0.1 M $KCHO_3$. Cyclic voltammograms were measured in non-Faradaic regions at the following scan rate as 5, 30, 50, 80, 100, 150, and 200 mV/s respectively. (a) CVs of the pristine 32 nm Cu; (b) CVs of the compressively strained 32 nm Cu; (c) CVs of the tensilely strained 32 nm Cu; (d) Determination of double-layer capacitance, in which the slope of the linear regressions of the data yields the double-layer capacitance of Cu overlayers as indicated in the figure.

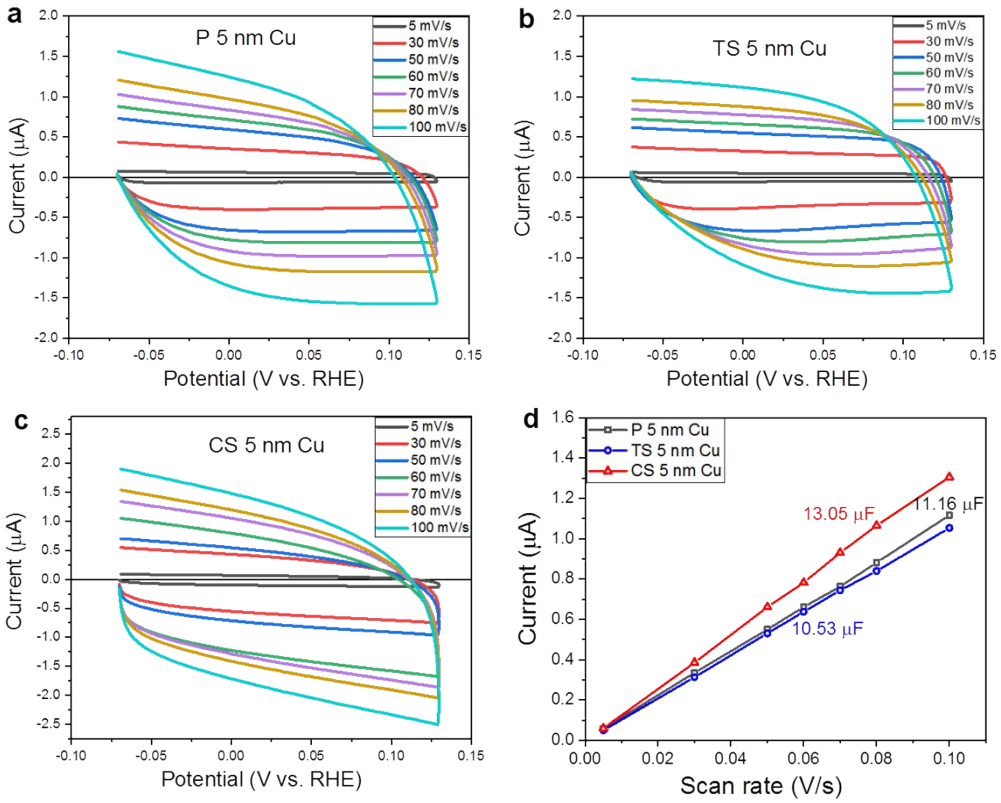

Figure S4. Double-layer capacitance measurements for determining the electrochemical active surface area for three state 5 nm Cu overlayers from voltammetry in CO_2 saturated 0.1 M $KCHO_3$. Cyclic voltammograms were measured in non-Faradaic regions. (a) CVs of the pristine 5 nm Cu; (b) CVs of the tensilely strained 5 nm Cu; (c) CVs of the compressively strained 5 nm Cu; (d) Determination of double-layer capacitance, in which the slope of the linear regressions of the data yields the double-layer capacitance of Cu overlayers as indicated in the figure.

Table S2. Double-layer capacitance, ECSA and roughness factor of Cu overlayers

	P 32 nm Cu	**CS 32 nm Cu**	**TS 32 nm Cu**	**P 5 nm Cu**	**CS 5 nm Cu**	**TS 5 nm Cu**
C_{DL}	23.37 μF	26.94 μF	21.46 μF	11.16 μF	13.05 μF	10.53 μF
ECSA	0.83 cm^2	0.96 cm^2	0.77 cm^2	0.40 cm^2	0.47 cm^2	0.38 cm^2
Roughness factor	2.08	2.40	1.93	1.00	1.18	0.95

Table S3. Total geometric current density, partial geometric current density toward CO_2RR and faradaic efficiencies of the main products of 32 nm pristine Cu after 60 minutes bulk electrocatalysis. CO-carbon monoxide, CH_4-methane, $HCOO^-$-formate, C_2H_4-ethylene, C_2H_5OH-ethanol, H_2-hydrogen.

E **(V vs. RHE)**	**Total current density J_{geo} (mA*cm^{-2})**	**CO FE (%)**	**CH_4 FE (%)**	**$HCOO^-$ FE (%)**	**C_2H_4 FE (%)**	**C_2H_5OH FE (%)**	**H_2 FE (%)**	**Total FE (%)**	**Partial current density for CO_2RR J_{CER} (mA*cm^{-2})**
-0.8	-3.82	25.18	0.33	17.67	2.10	0.38	50.83	96.49	-1.74
-0.9	-7.53	19.76	3.43	14.02	8.25	1.95	46.47	93.88	-3.57
-1.0	-11.58	15.10	17.84	6.52	15.26	2.62	37.06	94.40	-6.64
-1.1	-20.37	9.32	31.68	3.17	18.41	4.43	31.65	98.66	-13.65
-1.2	-29.17	5.02	42.76	2.03	12.89	2.32	32.18	97.2	-18.97
-1.3	-46.02	4.15	22.05	1.94	7.72	1.88	53.28	91.02	-17.37
-1.4	-72.83	3.43	7.80	1.65	5.43	1.21	72.53	92.05	-14.22

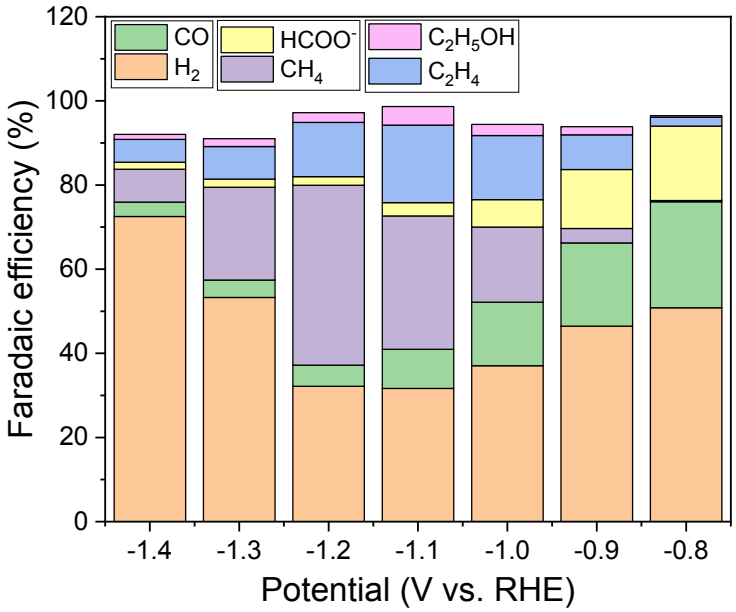

Figure S5. Faradaic efficiencies of hydrogen, carbon monoxide, methane, formate, ethylene and ethanol of 32 nm pristine Cu at different potentials shown in stacking columns.

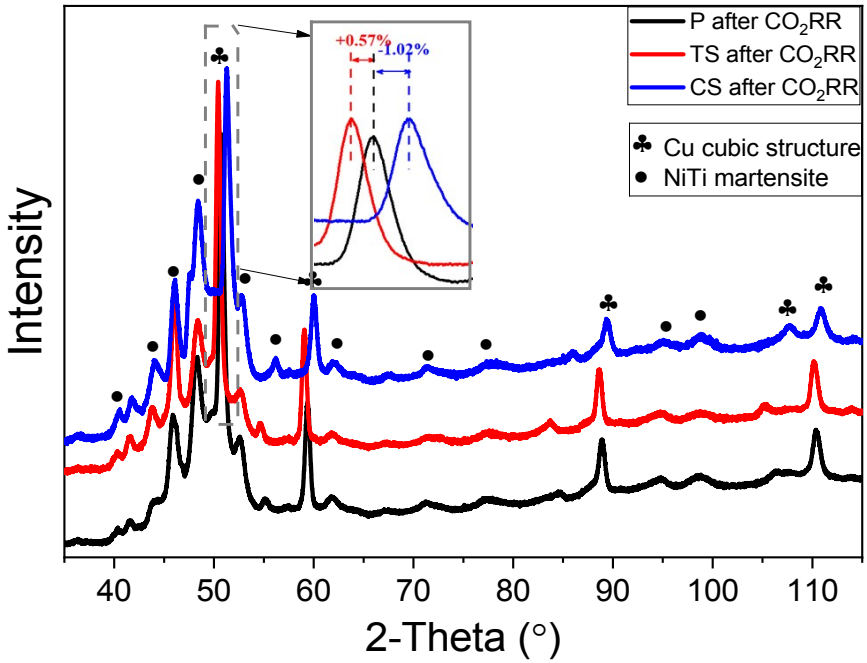

Figure S6. GIXRD profiles of 32 nm Cu/NiTi substrate samples under P, TS and CS states after CO_2 electroreduction reaction, and the enlargement of Cu-(111) diffraction peak was also shown inserted.

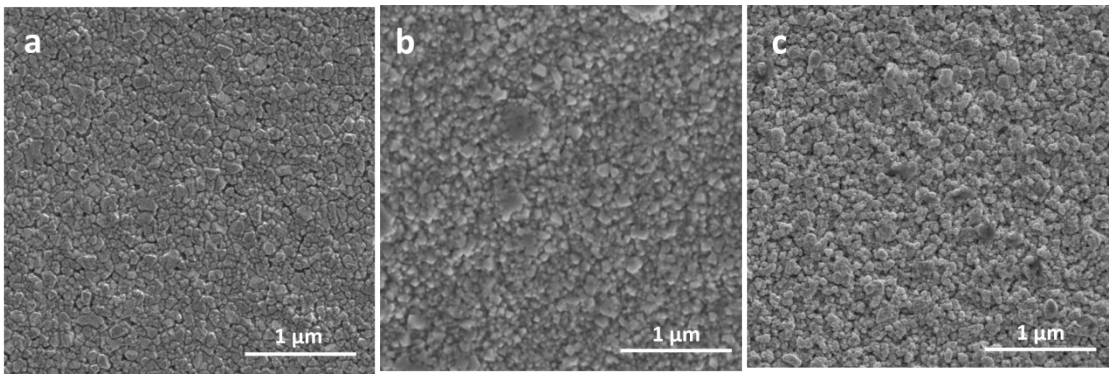

Figure S7. SEM images of the post-reaction 32 nm Cu /NiTi substrate samples in the state of (a) the pristine, (b) tensilely strained and (c) compressively strained.

Table S4. ECSA normalized total current density and faradaic efficiencies of the main products of pristine (P), tensile strained (TS), and compressive strained (CS) 32 nm Cu after 60 minutes bulk electrocatalysis. CO-carbon monoxide, CH_4-methane, $HCOO^-$-formate, C_2H_4-ethylene, C_2H_5OH-ethanol, H_2-hydrogen.

E **(V vs. RHE)**	**Sample**	**CO FE (%)**	**CH_4 FE (%)**	**$HCOO^-$ FE (%)**	**C_2H_4 FE (%)**	**C_2H_5OH FE (%)**	**H_2 FE (%)**	**Total FE (%)**	**Total current density J_0 ($mA*cm^{-2}$)**
-1.0	**P**	15.10	17.84	6.52	15.26	2.62	37.06	94.40	-5.58
	TS	16.34	19.03	8.81	15.83	2.21	35.82	98.04	-6.56
	CS	13.15	14.46	4.37	15.11	2.34	45.15	94.58	-4.42
-1.1	**P**	9.32	31.68	3.17	18.41	4.43	31.65	98.66	-9.82
	TS	11.12	35.73	5.93	19.82	4.15	25.03	101.78	-11.27
	CS	7.65	24.82	2.24	19.06	4.23	37.84	95.84	-7.59
-1.2	**P**	5.02	42.76	2.03	12.89	2.32	32.18	97.20	-14.06
	TS	5.78	50.64	3.85	14.04	2.17	23.07	99.55	-16.43
	CS	4.11	32.92	1.42	12.27	2.25	42.42	95.39	-10.76

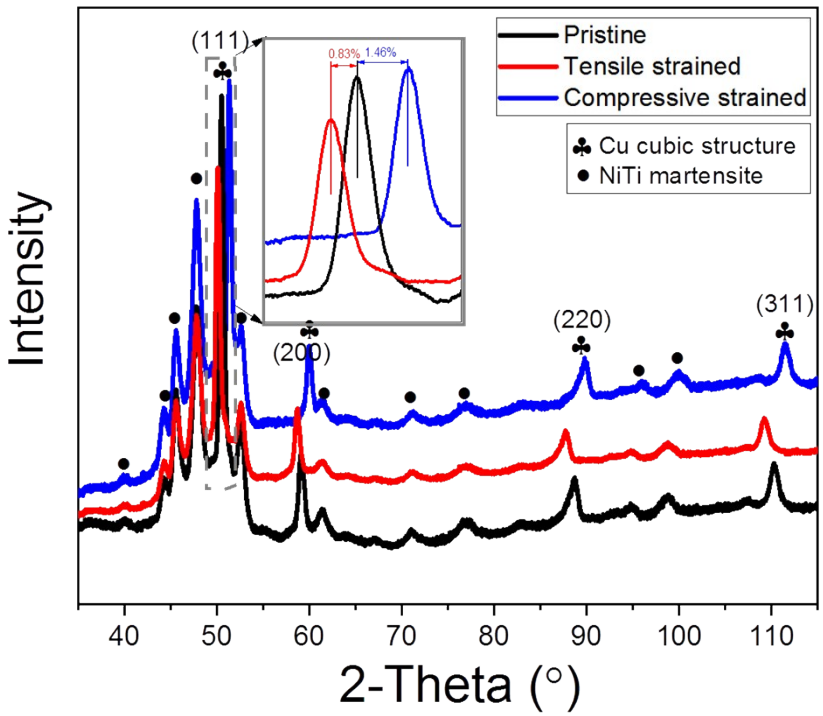

Figure S8. GIXRD pattern of 5 nm Cu/NiTi substrate sample under P, TS and CS states, and the enlargement of Cu-(111) diffraction peak was also shown inserted.

Table S5. Total current density and faradaic efficiencies of the main products of 5 nm pristine Cu overlayers after 60 minutes bulk electrocatalysis. CO-carbon monoxide, CH_4-methane, $HCOO^-$-formate, C_2H_4-ethylene, H_2-hydrogen.

E **(V vs. RHE)**	**Total current density *J* (mA*cm^{-2})**	**CO FE (%)**	**CH_4 FE (%)**	**$HCOO^-$ FE (%)**	**C_2H_4 FE (%)**	**H_2 FE (%)**	**Total FE (%)**	**Partial current density for CO_2RR J_{CER} (mA*cm^{-2})**
-0.8	-4.27	2.82	7.56	1.48	5.25	72.03	89.14	-0.73
-0.9	-8.91	2.739	8.29	1.43	5.42	73.43	91.30	-1.59
-1.0	-15.82	2.57	8.63	1.35	4.84	74.18	91.57	-2.75
-1.1	-23.07	2.46	9.03	1.28	3.97	75.02	91.76	-3.86
-1.2	-36.58	2.40	9.71	1.23	3.36	76.28	92.98	-6.11
-1.3	-58.2	2.25	10.03	1.22	2.79	77.05	93.34	-9.48
-1.4	-81.45	2.13	10.18	1.17	2.57	78.19	94.24	-13.07

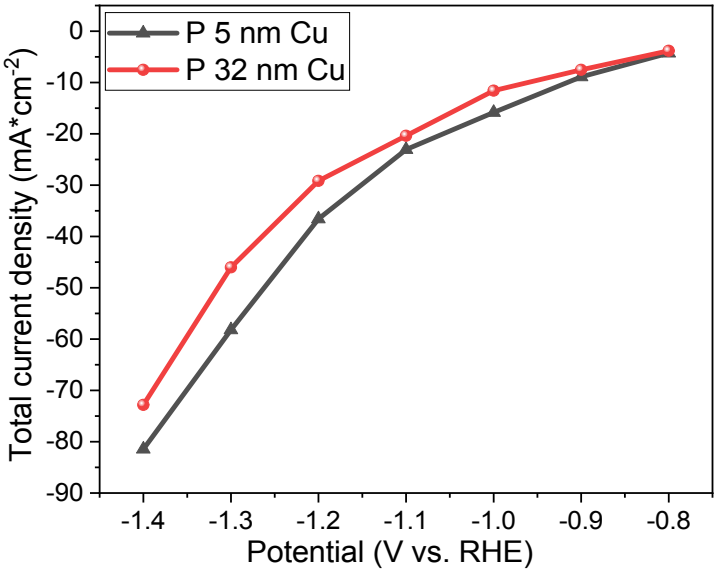

Figure S9. Comparison of total geometric current densities of the pristine 5 nm Cu and pristine 32 nm Cu overlayers as a function of cathodic potential in CO_2-saturated 0.1 M $KHCO_3$.

Table S6. Total current density and faradaic efficiencies of the main products of pristine (P), tensile strained (TS), and compressive strained (CS) 5 nm Cu after 60 minutes bulk electrocatalysis. CO-carbon monoxide, CH_4-methane, $HCOO^-$-formate, C_2H_4-ethylene, H_2-hydrogen.

E **(V vs. RHE)**	**Sample**	**CO FE (%)**	**CH_4 FE (%)**	**$HCOO^-$ FE (%)**	**C_2H_4 FE (%)**	**H_2 FE (%)**	**Total FE (%)**	**Total current density J_0 ($mA*cm^{-2}$)**
-1.0	**P**	2.57	8.63	1.35	4.84	74.18	91.57	-15.82
	TS	2.52	6.82	1.21	3.85	76.45	90.85	-18.09
	CS	4.61	9.37	1.71	5.18	59.49	80.36	-11.63
-1.1	**P**	2.46	9.03	1.28	3.97	75.02	91.76	-23.07
	TS	2.37	7.48	0.93	3.12	79.68	93.58	-26.88
	CS	4.85	10.06	1.58	4.27	65.03	85.79	-16.80
-1.2	**P**	2.40	9.71	1.23	3.36	76.28	92.98	-36.58
	TS	2.11	7.95	0.82	2.68	83.08	96.64	-41.34
	CS	4.26	11.49	1.54	3.91	68.31	89.51	-28.47

Table S7. Faradaic efficiencies of the main products of pristine (P), tensile strained (TS), and compressive strained (CS) 20 nm Cu and 7 nm Cu after 60 minutes bulk electrocatalysis when biased at -1.2 V. CO-carbon monoxide, CH_4-methane, $HCOO^-$-formate, C_2H_4-ethylene, H_2-hydrogen.

Cu Thickness (nm)	**Sample**	**CO FE (%)**	**CH_4 FE (%)**	**$HCOO^-$ FE (%)**	**C_2H_4 FE (%)**	**CO_2RR FE (%)**	**H_2 FE (%)**	**Total FE (%)**
20	**P**	3.40	37.26	1.87	13.15	55.68	37.03	92.71
	TS	3.78	44.91	2.02	14.03	64.74	32.86	97.60
	CS	3.11	27.43	1.69	13.02	45.25	42.71	87.96
7	**P**	3.06	18.28	1.04	5.23	27.61	61.22	88.83
	TS	2.81	15.35	0.97	4.96	24.09	66.42	90.51
	CS	4.17	22.14	1.20	5.42	32.93	53.08	86.01

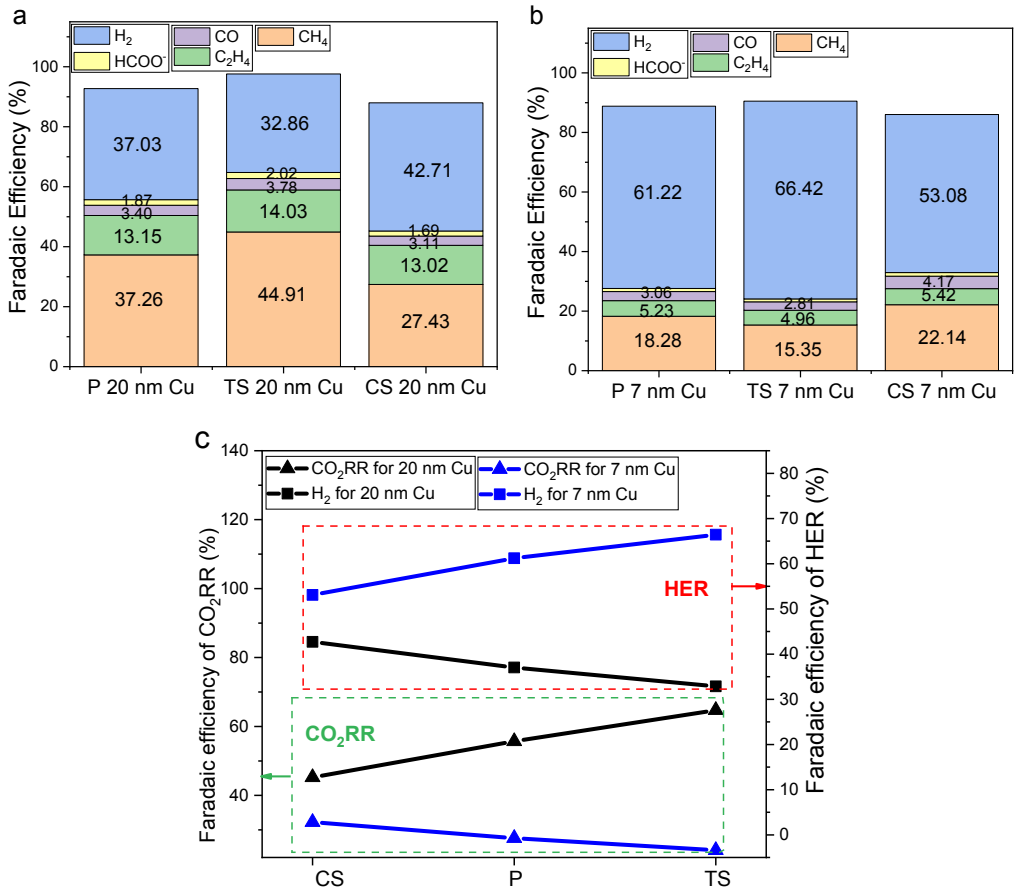

Figure S10. Strain effects on the Faradaic efficiencies of the main products of (a) 20 nm Cu overlayers, (b) 7 nm Cu overlayers and (c) total CO_2RR and HER of 20 nm and 7 nm Cu in comparison. The opposite strain effects on CO_2RR activity for 20 nm Cu and 7 nm Cu were similar to those observed for 32 nm Cu and 5 nm Cu as described in the text of article.

Table S8. DFT calculated results of d-band center and adsorption energies of main intermediates in CO_2RR on Cu (111) under different strain state.

	Pristine Cu (111)	**0.58% tensile-strain Cu (111)**	**-1.02% compressive-strain Cu (111)**
d band center	-2.273 eV	-2.247 eV	-2.324 eV
Adsorption energy of COOH*	1.302 eV	1.284 eV	1.338 eV
Adsorption energy of CO*	0.962 eV	0.956 eV	0.972 eV
Adsorption energy of CHO*	1.662 eV	1.649 eV	1.695 eV

Discussion on the correlation between free energy change ΔG and energy barrier Q for a single electron transfer reaction.

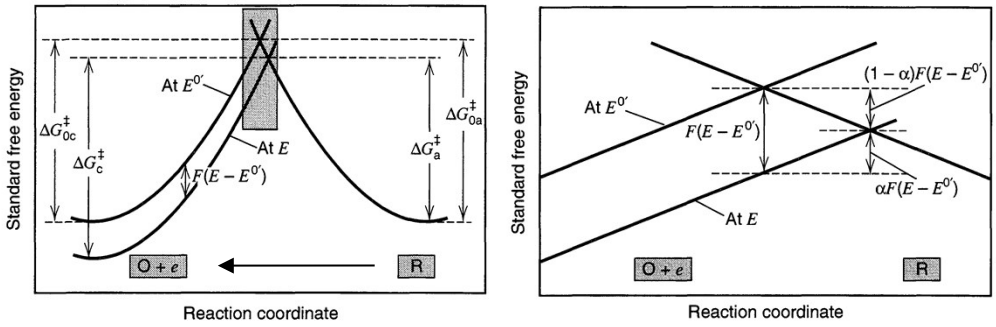

Considering a reaction of $O + e^{-1} \rightleftharpoons R$, when the potential changes with a positive ΔE from E^0 to E, the cathodic free energy profile dropped with $-F\Delta E = -F(E - E^0)$.

Then, for the anodic barrier,

$$\Delta G_{a}^{\neq} = \Delta G_{0a}^{\neq} - (1-\alpha)F(E - E^0) \quad \ldots\ldots\ldots\ldots\ldots\ldots\ldots\ldots (1)$$

for the cathodic barrier,

$$\Delta G_{c}^{\neq} = \Delta G_{0c}^{\neq} + \alpha F(E - E^0) \quad \ldots\ldots\ldots\ldots\ldots\ldots\ldots\ldots\ldots\ldots (2)$$

The reaction would go backward, that was R $\rightarrow O + e^{-1}$.

Thus, the reaction kinetic barrier was:

$$Q = \Delta G_{a}^{\neq} = \Delta G_{0a}^{\neq} - (1-\alpha)F(E - E^0) \quad \ldots\ldots\ldots\ldots\ldots\ldots (3)$$

From (3), we get: $$F(E - E^0) = \frac{1}{1-\alpha}(\Delta G_{0a}^{\neq} - Q) \quad \ldots\ldots\ldots\ldots\ldots\ldots\ldots (4)$$

And the reaction free energy change was:

$$\Delta G = \Delta G_{a}^{\neq} - \Delta G_{c}^{\neq} \quad \ldots\ldots\ldots\ldots\ldots\ldots\ldots\ldots\ldots\ldots\ldots\ldots (5)$$

From (1) and (2), (5) could be expressed by:

$$\Delta G = \Delta G_{0a}^{\neq} - (1-\alpha)F(E - E^0) - \Delta G_{0c}^{\neq} - \alpha F(E - E^0)$$

$$\Delta G = \Delta G_{0a}^{\neq} - \Delta G_{0c}^{\neq} - F(E - E^0) \quad \ldots\ldots\ldots\ldots\ldots\ldots\ldots (6)$$

Take (4) into (6) and obtain that:

$$\Delta G = \frac{Q}{1-\alpha} - \Delta G_{0c}^{\neq} - \frac{\alpha}{1-\alpha}\Delta G_{0a}^{\neq} \quad \ldots\ldots\ldots\ldots\ldots\ldots\ldots\ldots\ldots\ldots (7)$$

Where, α is transfer coefficient ($0 \leq \alpha \leq 1$) that is a measure of the symmetry of the energy profiles. In most system, $\alpha\ turns$ out lie between 0.3 and 0.7, and can usually be approximated by 0.5 in the absence of actual measurements. And $\Delta G_{0c}^{\neq}\ and\ \Delta G_{0a}^{\neq}$ are cathodic and anodic activation energies at the equilibrium potential E^0.

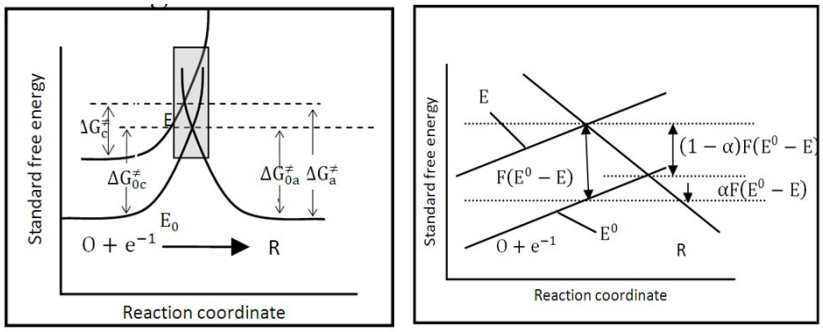

Again, considering a reaction for $O + e^{-1} \rightleftharpoons R$, when the potential changes with a negative ΔE from E^0 to E, the cathodic free energy profile lifted with $-F\Delta E = -F(E - E^0)$.

Then, for the anodic barrier,

$$\Delta G_a^{\neq} = \Delta G_{0a}^{\neq} + (1-\alpha)F(E^0 - E) \quad \ldots\ldots\ldots\ldots\ldots\ldots\ldots\ldots (8)$$

for the cathodic barrier,

$$\Delta G_c^{\neq} = \Delta G_{0c}^{\neq} - \alpha F(E^0 - E) \quad \ldots\ldots\ldots\ldots\ldots\ldots\ldots\ldots\ldots\ldots (9)$$

The reaction would go forward, that was $O + e^{-1} \rightarrow$ R.

Thus, the reaction kinetic barrier was:

$$Q = \Delta G_c^{\neq} = \Delta G_{0c}^{\neq} - \alpha F(E^0 - E) \quad \ldots\ldots\ldots\ldots\ldots\ldots\ldots\ldots (10)$$

According to (10), one can get that:

$$F(E - E^0) = \frac{1}{\alpha}(\Delta G_{0c}^{\neq} - Q) \quad \ldots\ldots\ldots\ldots\ldots\ldots\ldots\ldots (11)$$

And the reaction free energy change was:

$$\Delta G = \Delta G_c^{\neq} - \Delta G_a^{\neq} \quad \ldots\ldots\ldots\ldots\ldots\ldots\ldots\ldots\ldots\ldots (12)$$

From (8) and (9), (12) was expressed with:

$$\Delta G = \Delta G_{0c}^{\neq} - \alpha F(E^0 - E) - \Delta G_{0a}^{\neq} + (\alpha - 1)F(E^0 - E)$$

$$\Delta G = \Delta G_{0c}^{\neq} - \Delta G_{0a}^{\neq} - F(E - E^0) \quad \text{..... (13)}$$

Take (11) into (13), obtained:

$$\Delta G = \frac{Q}{\alpha} - \Delta G_{0a}^{\neq} + (1 - \frac{1}{\alpha})\Delta G_{0c}^{\neq} \quad \text{..... (14)}$$

Where, α is transfer coefficient ($0 \leq \alpha \leq 1$) which is a measure of the symmetry of the energy profiles. In most system, $\alpha\ turns$ out lie between 0.3 and 0.7, and can usually be approximated by 0.5 in the absence of actual measurements. And $\Delta G_{0c}^{\neq}\ and\ \Delta G_{0a}^{\neq}$ are cathodic and anodic activation energies at the equilibrium potential E^0.

In conclusion, for single electron transfer reaction including the anodic reaction (R $\rightarrow O + e^{-1}$) and the cathodic reaction ($O + e^{-1}\rightarrow$ R), reaction free energy change ΔG and kinetic barrier Q are positive correlated with a coefficient of $\frac{1}{1-\alpha}$ or $\frac{1}{\alpha}$ respectively.

Discussion on the correlation between free energy change ΔG and energy barrier Q for an electrocatalytic reaction.

Considering a general electroreduction reaction of: A* + H^+ + e^- ⇌ AH*. The computational hydrogen electrode (CHE) mode was coupled with energetics from DFT calculations to account for the chemical potential of proton-electron pairs ($H^+ + e^-$). According to CHE mode, the free energy change was:

$$\Delta G = G(AH^*) - G(A^*) - \left[{}^1/_2 G(H_2) - eU\right] \quad \text{..... (1)}$$

For a limiting step, $G(AH^*)\ and\ G(A^*)$ were constant, so

$$\Delta G = a + eU \quad \text{..... (2)}$$

where $a = G(AH^*) - G(A^*) - \left[{}^1/_2 G(H_2)\right]$.

According to the transferable method developed by Michael J. Janik et al [], the potential-dependent energy barrier *Q* was obtained by considering a two-step process consisting of a reductive adsorption step of A* + H^+ + e^- ⇌ A* + H* and a chemical reaction of A* + H* ⇌ AH*, thus:

$$Q = Q(U^0) + e\beta'(U - U^0) \quad \text{..... (3)}$$

Where U^0 was the equilibrium potential for the reductive adsorption step, β' is an effective symmetry factor of free energy diagram, which was approximated by $\beta' = \beta + (\mu_{TS} - \mu_{reactant})/d$. Where β denotes a reaction symmetry factor, similar to a BEP coefficient as it denoted the relationship between the activation barrier change and the reaction energy change. β' was positive, typically between 0 and 1. According to Eq. (3):

$$Q = Q(U^0) + e\beta'U - e\beta'U^0 = b + e\beta'U \quad \text{..... (4)}$$

where $b = Q(U^0) - e\beta'U^0$. According to (2) and (4),

$$\Delta G = a + \frac{1}{\beta'}Q - \frac{b}{\beta'} = \frac{1}{\beta'}Q + c \quad \text{..... (5)}$$

Where $c = a - \frac{b}{\beta'} = G(AH^*) - G(A^*) - \left[\frac{1}{2}G(H_2)\right] - \frac{Q(U^0)}{\beta'} + eU^0$. Thus, seen from Eq. (5), ΔG and Q was positive correlated.

It should be noticed that for a RDS at 0 V vs. RHE, the reaction is generally uphill with $\Delta G > 0$. It means that the reaction cannot happen without applying a negative potential (overpotential), the minimum of which was known as the limiting potential U_L.

X. Nie, M. R. Esopi, M. J. Janik, A. Asthagiri, Selectivity of CO_2 reduction on copper electrodes: The role of the kinetics of elementary steps. Angew. Chem. Int. Ed. 2013, **52**, 2459−2462.